1   Supporting Information for

2   **Monoethanolamine Decay Mediated by Photolysis of Nitrate in Atmospheric**

3   **Particles: A Brown Carbon and Organic Phase Formation Pathway**

4   *Xiaomeng Tian[1,2], Ruifeng Zhang[1,2], Bo Wei,[1,3] Yalin Wang,[4] Yongjie Li, [4] and Chak K.*

5   *Chan [,1,2]**

6   [1]School of Energy and Environment, City University of Hong Kong, Tat Chee Avenue,

7   Kowloon, Hong Kong, China

8   [2]City University of Hong Kong Shenzhen Research Institute, Shenzhen 518057, China;

9   [3]Environment Research Institute, Shandong University, Qingdao, 266237, PR China

10   [4]Department of Civil and Environmental Engineering, and Centre for Regional Oceans,

11   Faculty of Science and Technology, University of Macau, Macau 999078, China

12   *Corresponding author

13   Email: chak.k.chan@cityu.edu.hk

14   Telephone: +(852)-3442-5593.

15   Fax: +(852)-3442-0688

16

17   **Text S1** Ion Chromatography (IC) measurement for Product Characterization.

18   **Text S2** Sample pre-treatment by solid phase extraction (SPE)

19   **Text S3** UHPLC-MS measurement method

20   **Text S4** Determination of bisulfate to sulfate Raman peak area and molar ratio of

21   particles in photolysis experiments

22   **Text S5** DFT calculation

function of time of irradiation. The phase change of the 4:0.5:1:3 particles at 40%RH is highlighted in the dashed box.

Fig. S8. Morphology of the 4:0.5:1:3 particles at 85% RH after 24hr irradiation.

Fig. S9. The 4:0.5:1:3 particles on the substrate before the experiment (a), after 24hr irradiation (b) and continually supplying air without UV irradiation for another 12 hr (c) at 85%RH.

Fig. S10. Raman spectra for the liquid phase of the studied particle (a) and a neighboring particle(b) after 24hr UV irradiation. During the 24hr irradiation, no Raman laser exposure was given to particles. Raman spectra for the particle at 0hr before UV irradiation were plotted as the reference.

Fig. S11. (a) Freshly made solution by mixing MEA, NH_2CHO, CHOCHO, NH_2CH_2COOH, Na_2SO_4, $(NH_4)_2SO_4$ and H_2SO_4. (b) Same solution after 3 days in dark.

Fig. S12. Raman spectra for the particle made by the solution in Fig. S11(b).

Fig. S13. (a) Morphology of particles made from the solution in Fig. S11(b); (b) Morphology of particles made from the solution in Fig. S11(b) after 24hr UV irradiation. $NaNO_3$ was added to the solution before making particles.

Fig. S14. (a) Detected Raman signals in the organic phase at 24 hr irradiation of the 4:0.5:1:3 particles at 85% RH for the second scan and in the organic phase from BrC photolysis. Raman peaks of the organic phase in each spectrum were highlighted in red in (b) and (c).

Fig. S15. Detected Raman signals in oxamide and in the organic phase after 24 hr irradiation of the 4:0.5:1:3 particles at 85% RH for the second scan. Raman peaks attributed to oxamide were highlighted in red.

70 **Fig. S16.** Changes in morphologies of the 4:0.5:1:3 particles at 80%RH (a) Particles

71 before the experiment; (b) particles after one cycle of day-night (12hr UV+12hr dark);

72 (c) particles after the one cycle of day-night and a day (12hr UV+12hr dark +12hr UV);

73 (d) particles after the one cycle of day-night and a day + 8hr dark, arrows indicating the

74 organic phase in particles, photo was extended by merging two photos(e) particles after

75 3 cycle of day-night.

76 **Table S1.** Raman calibration experiments using different NH_4Cl: H_2SO_4: Na_2SO_4

77 solutions to determine $A(HSO_4^-)/A(SO_4^{2-})$ as a function of pH for MEA oxidation

78 experiments. Noted that the SO_4^{2-} mole fraction of the solute in MEA: H_2SO_4: $NaNO_3$:

79 HNO_3 = 4:1:1:3 and 4:0.75:1:3 are 1/11 and 0.75/10.25 respectively. All calibration

80 experiments were carried out at 70%RH.

81 **Table S2.** Compound found in MS with the m/z values and structure.

82

83 **Text S1 Ion Chromatography (IC) measurement for Product Characterization.** A

84 Dionex ICS-1100 system was used for product characterization after photolysis.

85 Sample particles collected on the substrate after the photolysis were dissolved with

86 0.5mL DI water. Blank samples were made by dissolving sample particles on the

87 substrate without irradiation. For cation analysis, the IC system was equipped with an

88 IonPac CS12A analysis column and an IonPac CG12A guard column. Samples were

89 eluted with 20 mM methanesulfonic acid (MSA) at 1 mL min^{-1}. The retention time at

90 ~5.7min was assigned to NH_4^+ by comparing it with NH_4^+ in the NH_4Cl standard

91 solution. For anion analysis, the IC system was equipped with an IonPac AS15 analysis

92 column and an IonPac AG15 guard column. Samples were eluted with 38mM NaOH at

93 1.2 mL min^{-1}. The retention time at ~3.3 min was assigned to formate by comparing

94 and comparing with formate in sodium formate standard solution.

95 **Text S2 Sample pre-treatment by solid phase extraction (SPE).** Before MS analysis,

96 SPE was performed on all the samples using SPE cartridges (HLB, 60 mg, 3cc, 30 μm,

97 Waters) to desalt or remove bisulfate and sulfate ions that may damage the LC column.[1]

98 The SPE procedure was used as follows.[1,2] First, the SPE cartridge was activated and

99 conditioned by rinsing with 1 mL HPLC grade MeOH and 1 mL deionized water, then

100 drained by an external pump after pre-washing. A volume of 1 mL of sample was added

101 to the SPE tube. The tube was then washed with 1 mL 5% MeOH solution to remove

102 the bisulfate and sulfate ions. Then the SPE tube was dried by flushing air through the

103 cartridge using an air pump. Organic compounds adsorbed on the SPE column were

104 eluted using 1mL HPLC grade acetonitrile for Orbitrap analysis.

105 **Text S3 UHPLC-MS measurement method**. Thermo Scientific Dionex Ultimate

106 3000 UHPLC system with a Thermo Q Exactive Focus Orbitrap-Quadrupole Mass

107 Spectrometer was used to characterize the reaction products.[1]

108   The separation of products was conducted using a Shim-pack GIST C18 column

109 (3 μm, 2.1 mm × 100 mm; Shimadzu). The column oven was held at 30 °C, and the

110 autosampler was cooled at 10°C. The injection volume was set to 10 μL. The binary

111 mobile phase consisted of A (water) and B (acetonitrile). The gradient elution was

112 performed at a flow rate of 0.3 mL/min: 0-4 min, linear increase to 3% eluent B; 4-

113 7min, linear increase to 50% eluent B; 7-8 min, hold 50% eluent B; 8-10 min, linear

114 increase to 100% eluent B, and then stop at 10 min.

115 **Text S4 Determination of bisulfate to sulfate Raman peak area and molar ratio of**

116 **particles in photolysis experiments.** Species concentrations are reflected by Raman

117 peak areas.[2] In this study, we used SO_4^{2-} as the internal standard to eliminate the effect

118 of Raman laser intensity change in the measurement of Raman peak areas. In particular:

$$\frac{[MEA]}{[SO_4^{2-}]} = \frac{S_{MEA}\, A(MEA)}{S_{sulfate}\, A(SO_4^{2-})}$$

119   (S1)

$$\frac{[NO_3^{-}]}{[SO_4^{2-}]} = \frac{S_{nitrate}\, A(NO_3^{-})}{S_{sulfate}\, A(SO_4^{2-})}$$

120   (S2)

121 where S_{MEA}, $S_{sulfate}$ and $S_{nitrate}$ denote the slope in the correlation between concentration

122 and peak area of MEA, SO_4^{2-} and NO_3^{-} respectively.

123   However, pH affects the equilibrium of $SO_4^{2-} + H^+ = HSO_4^-$, which changes

124 $[SO_4^{2-}]$ during the photooxidation reactions of MEA. Besides, NO_3^- and HSO_4^- Raman

125 peaks are overlapped at ~1050cm^{-1}. Hence, the determination of n(MEA) and n(NO_3^-)

126 need to incorporate the presence of bisulfate (HSO_4^-), especially at low pH. n(MEA)

127 and n(NO_3^-) should be normalized by the total amount of SO_4^{2-} containing species

128 (n(SO_4^{2-}) +n(HSO_4^-)).

129   To address the influence of pH changes to the distribution of HSO_4^- and SO_4^{2-},

130 we first developed empirical fits of the temporal changes of pH of the droplets from the

131 MEA oxidation experiments (Fig. S4a and b).

132 pH (MEA: H_2SO_4: $NaNO_3$: HNO_3=4:1:1:3) = -0.0007t^3 + 0.0025t^2 + 0.1772t + 0.1586

133 (S3)

134 pH (MEA: H_2SO_4: $NaNO_3$: HNO_3=4:0.75:1:3) = 0.0769t + 0.905   (S4)

135 t is the photolysis time in hours in the above equations.

136   Then, we estimated $A(HSO_4^-)/A(SO_4^{2-})$ and n(HSO_4^-)/n(SO_4^{2-}) as particle pH

137 changes using NO_3^- - free solutions at different pH values to avoid the overlapping of

138 NO_3^- and HSO_4^- peaks. It would be ideal to use MEA salts for these Raman calibration

139 experiments. However, their thermodynamic database is very limited in E-AIM. We

140 therefore used inorganic reagents to prepare the solutions. As listed in Table S1, NH_4Cl

141 (99.5%, Sigma-Aldrich), H_2SO_4 (95.0%, Acros Organics), and Na_2SO_4 (95.0%, Acros)

142 were used to produce solutions of a range of pH (estimated by E-AIM). Each solution

143 was atomized to produce particles for Raman measurements at 70%RH. Raman peaks

144 at ~979 and 1050 cm^{-1} were attributed to the $v(SO_4^{2-})$ and $v(HSO_4^-)$, respectively. The

145 pH of particles and $n(HSO_4^-)/n(SO_4^{2-})$ were calculated by E-AIM and listed in Table

146 S1.

147   We also consider the possibility that the SO_4^{2-} mole fraction of the solute

148 influences the distribution of HSO_4^- and SO_4^{2-} due to ionic interactions. Hence, two sets

149 of solutions were produced with SO_4^{2-} mole fraction of the solutes corresponding to the

150 initial value of the particles at MEA: H_2SO_4: $NaNO_3$: HNO_3 = 4:1:1:3 and 4:0.75:1:3.

151 Although MEA and NO_3^- were continuously depleted and new products were formed

152 during the photolysis experiment, we assume that the SO_4^{2-} mole fraction of the solute

153 was approximately constant in the first few photolysis hours. Fig. S4(c) and (d) describe

154 the $A(HSO_4^-)/A(SO_4^{2-})$ and $n(HSO_4^-)/n(SO_4^{2-})$ as a function of particle pH, respectively.

155 Note that the MEA: H_2SO_4: $NaNO_3$: HNO_3=4:1:1:3 and 4:0.75:1:3 particles show the

156 same trends within the measured pH range, suggesting that the trends of $A(HSO_4^-$

157 $)/A(SO_4^{2-})$ and $n(HSO_4^-)/n(SO_4^{2-})$ are independent of the SO_4^{2-} mole fraction of the

158 solute within the bounds of these compositions. The data from the two sets of

159 compositions were hence combined to obtain empirical fits (Eqn S5-6).

160 $A(HSO_4^-)/A(SO_4^{2-}) = -0.2613(pH)^3 + 0.9847(pH)^2 - 1.3477\ pH + 0.7169$

161 (S5)

162 $n(HSO_4^-)/n(SO_4^{2-}) = -0.2341(pH)^3 + 0.9857(pH)^2 - 1.5894pH + 0.9955$

163 (S6)

164   With $n(HSO_4^-)/n(SO_4^{2-})$ as a function of pH of oxidation time known, we

165 normalized [MEA] and [NO$_3^-$] by the total concentration of SO$_4^{2-}$ containing species

166 ([SO$_4^{2-}$]$_{total}$ = [HSO$_4^-$]+[SO$_4^{2-}$]), which is a constant irrespective of pH as described in

167 Eqn S7-8.

168
$$\frac{[MEA]}{[SO_4^{2-}]_{total}} = \frac{[MEA]}{[SO_4^{2-}](1 + \frac{[HSO_4^-]}{[SO_4^{2-}]})} = \frac{S_{MEA}\,A(MEA)}{S_{sulfate}\,A(SO_4^{2-})\left(1 + \frac{n(HSO_4^-)}{n(SO_4^{2-})}\right)}$$

169 (S7)

170
$$\frac{[NO_3^-]}{[SO_4^{2-}]_{total}} = \frac{[NO_3^-]}{[SO_4^{2-}](1 + \frac{[HSO_4^-]}{[SO_4^{2-}]})} = \frac{S_{MEA}\,A(MEA)}{S_{sulfate}\,A(SO_4^{2-})\left(1 + \frac{n(HSO_4^-)}{n(SO_4^{2-})}\right)}$$

171 (S8)

172   In the above equation, $A(SO_4^{2-})$ is the measured SO$_4^{2-}$ peak area in Raman,

173 $A(SO_4^{2-})$ [HSO$_4^-$]/[SO$_4^{2-}$] is the calculated peak area when using SO$_4^{2-}$ peak area to

174 reflect the concentration of HSO$_4^-$. Thus, $A(SO_4^{2-}) \times$ (1+ [HSO$_4^-$]/[SO$_4^{2-}$]) indicates the

175 peak areas of the total SO$_4^-$ containing species([HSO$_4^-$] + [SO$_4^{2-}$]), if all HSO$_4^-$ existed

176 as SO$_4^{2-}$. $A(NO_3^-)$ is the peak attributable to NO$_3^-$, after subtraction of overlapping

177 $A(HSO_4^-)$ from the measured Raman peak at 1000-1100 cm^{-1}, where the overlapping

178 $A(HSO_4^-)$ can be obtained from Eqn S5. The total concentration of SO$_4^{2-}$ containing

179 species is described as [SO$_4^{2-}$] (1+ [HSO$_4^-$]/[SO$_4^{2-}$]). Noted that [HSO$_4^-$]/[SO$_4^{2-}$] =

180 $n(HSO_4^-)/n(SO_4^{2-})$. At the low pH, with the coexistence of SO$_4^{2-}$ and HSO$_4^-$, n(HSO$_4^-$

181)/n(SO$_4^{2-}$) at any photolysis time can be estimated by combining Eqn(S3-4 and 6).

182   Eqns S7 and S8 ultimately give n(MEA)and n(NO$_3^-$) normalized to the n(SO$_4^{2-}$

183)$_{total}$ as a function of pH. To facilitate the analysis of the decay rate of MEA and NO$_3^-$,

184 we further normalize n(MEA) and n(NO$_3^-$) to their respective initial value (Fig. 2 in the

185 main text and Fig. S2 in the supporting information) as below:

$$\frac{n(NO_3^-)_t}{n(SO_4^{2-})(1+\frac{n(HSO_4^-)}{n(SO_4^{2-})})_t} \Bigg/ \frac{n(NO_3^-)_0}{n(SO_4^{2-})(1+\frac{n(HSO_4^-)}{n(SO_4^{2-})})_0} = \frac{n(NO_3^-)_t}{n(NO_3^-)_0}$$

186

187 (S9)

$$\frac{n(MEA)_t}{n(SO_4^{2-})(1+\frac{n(HSO_4^-)}{n(SO_4^{2-})})_t} \Bigg/ \frac{n(MEA)_0}{n(SO_4^{2-})(1+\frac{n(HSO_4^-)}{n(SO_4^{2-})})_0} = \frac{n(MEA)_t}{n(MEA)_0}$$

188

189 (S10)

190 **Text S5 DFT calculation.** All of the electronic structure calculations were conducted

191 using the Gaussian 16 program[3] employing the M06–2X[4] method with the 6−31+G(d,p)

192 basis set. The vibrational frequencies at the same level were used to verify all stationary

193 points as either the transition state (TS, only one imaginary frequency) or the minima

194 (zero imaginary frequency). The reaction pathways were confirmed by intrinsic

195 reaction coordinate (IRC) analysis. The single point energies of the optimized structures

196 were further calculated with the 6−311++G(3df,2p) basis set. The continuum solvation

197 model 'SMD' was used to determine the solvent effect of water.[5]

198 **Text S6 Proposed mechanism of MEA oxidation during NO$_3^-$ Photolysis.** MEA

199 oxidation forms peroxide radical (NH$_2$CH$_2$CH(OO·)OH) in the presence of O$_2$, and it

200 further forms NH$_2$CH$_2$CHO,[6,7] as shown in Step 1 in Fig. 3 and Fig. S6. NH$_2$CH$_2$CHO

201 was subsequently oxidized to form NH$_2$CH$_2$COOH (steps 2-2, 16).[8,9] Interestingly, the

202 α-H atom in NH$_2$CH$_2$CHO seems to be activated and further gives NH$_2$COCHO and

203 CHOCHO (Steps 2-3 and after). Even though NH$_2$CH$_2$CHO is more likely to exist in

204 the protonated form as NH$_3^+$CH$_2$CHO under the experimental pH condition, the two

205 adjacent electron pulling groups (-NH$_3^+$, -CHO) may deactivate the α-H atom.

206 However, it was reported that Na^+ could form a stable bidentate ligand with

207 NH_2CH_2COOH,[10] and Na^+ exhibits a stronger binding affinity with amide than

208 NH_2CH_2COOH.[11] Sodicated and protonated NH_2CH_2CHO were both found in the

209 UHPLC-MS analysis, as shown in Table S2. Thus, we propose a pentacyclic

210 intermediate in the oxidation of NH_2CH_2CHO, where Na^+ binds as the bidentate ligand

211 of $-NH_2$ and $-CHO$ on NH_2CH_2CHO (step 2-3). Chelation of Na^+ to $-NH_2$ shielded the

212 protonation of $-NH_2$, and shared the electron density with $-NH_2$ and $-CHO$, thus

213 reducing the electron pulling effect from the two adjacent groups when compared with

214 $NH_3^+CH_2CHO$. Besides, a steric benefit of pentacyclic structure may facilitate the OH

215 radical attack to $-CH_2-$. As a result, NH_2COCHO (step 11-1) and $CHOCHO$ (steps 11-

216 2, 13) were formed.

217   Through the reaction steps 2-1 and 3, fragmentation reaction is initiated by H

218 abstraction and O_2 addition to the $-CHO$ group in the presence of NO (from NO_3^-

219 photolysis) or RO_2 radicals(step 2-1 in Fig. S6), and subsequent formation of the amino

220 alkyl radical ($NH_2CH_2\cdot$) and CO_2.[12,13] $NH_2CH_2\cdot$ can react with O_2 and OH radical via

221 steps 4-1 and 4-2 to form amino peroxyl radical ($NH_2CH_2OO\cdot$)[14] and amino methanol

222 (NH_2CH_2OH),[15] respectively. $NH_2CH_2OO\cdot$ can further form amino alkoxy

223 radical(($NH_2CH_2O\cdot$, step 5-1) or react with NO to form amino nitrooxy

224 ($NH_2CH_2ONO_2$) (step 5-2).[16,17] Although the photodegradation of the so-formed

225 $NH_2CH_2ONO_2$ to $NH_2CH_2O\cdot$(step 6) has been proposed,[16] it is kinetically unfavorable

226 with a relatively high ΔG of 34.83 kcal/mol based on our calculation. NH_2CHO can be

227 formed through three pathways via the oxidation of $NH_2CH_2O\cdot$ (step 7-1),

228 $NH_2CH_2ONO_2$ (step 7-2), and NH_2CH_2OH (step 8).[13,15] NH_2CHO will ultimately go

229 through further acid-catalyzed hydrolysis to form HCOOH and NH_4^+(step 9-1, 10)[18,19]

230 or be oxidized to form CO_2 (step 9-2).

231 **Text S7 Proposed formation pathway for water-soluble BrC** To verify the BrC

232 formation potential of MEA and its oxidation products, a dark experiment of the bulk

233 solution without NO_3^- was performed to simulate the particle aging after MEA was

234 oxidized. Based on the MEA oxidation pathway shown in Fig. 3 in the main text, we

235 assume that half of MEA was oxidized, from which one half-formed CHOCHO and

236 NH_2CH_2COOH without C-C bond cleavage, and another half-formed NH_2CHO and

237 NH_4^+ by fragmentation. We prepared a solution stoichiometrically with MEA

238 (0.02mol), CHOCHO (0.01mol), NH_2CH_2COOH (0.01mol), NH_2CHO (0.01mol), and

239 Na_2SO_4 (0.005mol), $(NH_4)_2SO_4$ (0.01mol), then added H_2SO_4 to adjust the pH to ~4,

240 which corresponds to the particle pH value measured after the photolysis (Fig. 2). It

241 should be noted that the browning of aqueous particle phases only takes minutes to

242 hours while that of the aqueous bulk solution takes days.[20] After three days in the dark,

243 the solution turned brown, as shown in Fig. S11. Particles were made from the browned

244 solution and scanned by Raman spectroscopy. As shown in Fig. S12, the Raman spectra

245 for the particles also exhibited an enhanced background. Similar to the particulate MEA

246 oxidation experiment, the background intensity decreased after each successive Raman

247 scan within 1 minute, indicating that the BrC was photobleached by the 532nm laser.

248 **Text S8 Particulate MEA degradation mediated by NO_3^- photolysis under**

249 **atmospherically relevant conditions.** Based on the experimental room temperature

250 (22± 2℃), we consider the typical meteorological conditions in spring and autumn in

251 southern China, and set the simulation RH correspondingly at 80%RH.[21] In our

252 previous study about the reactive uptake of MEA by H_2SO_4 particles, we found that

253 under elevated RH conditions, MEA could effectively partition into acidic particles and

254 completely neutralize the H_2SO_4 particles within 1hr.[22] Thus, the fully neutralized

255 4:0.5:1:3 particles were used as the model particles to simulate the particulate MEA

256 degradation mediated by NO_3^- photolysis. Note that the photon flux received by

257 particles was $\sim 2 \times 10^{15}$ photons cm^{-2} s^{-1}, which is comparable with the intensity received

258 under the sunlight ($\sim 3.5 \times 10^{15}$ photons cm^{-2} s^{-1}) in spring and autumn despite the

259 irradiation wavelength difference.[21] However, previously, in the presence of OH radical

260 scavenger (glyoxal), it was found that the produced OH radical concentration is $\sim 10^{-15}$M, which falls in the range of the measured OH radical concentration (0.1-6×10^{-15}M)

262 in the reported field study.[23] Under the same RH and UV irradiation intensity, $[NO_3^-]$

263 and [MEA] were calculated as 4.26M,[24] which is coincidentally same as the $[NO_3^-]$ and

264 [glyoxal] used in the previous study. Although the OH radical scavenger is different,

265 the produced OH radical concentration should be similar. Therefore, we accepted the

266 same UV irradiation intensity used in the previous study to produce a comparable

267 concentration of OH radical. The irradiation time was set as 12hr, which is the same as

268 the sunshine duration in spring and autumn in southern China, which can be found in

269 CMDC (http://data.cma.cn/en). We simulated 12:12 hr of day and night cycle by

270 having 12hr UV irradiation+12hr dark to check the time of the organic phase formation

271 in the MEA-containing particles. To avoid the influence of the photo-bleach given by

272 the Raman laser, during the simulation, no Raman scan was applied to the studied
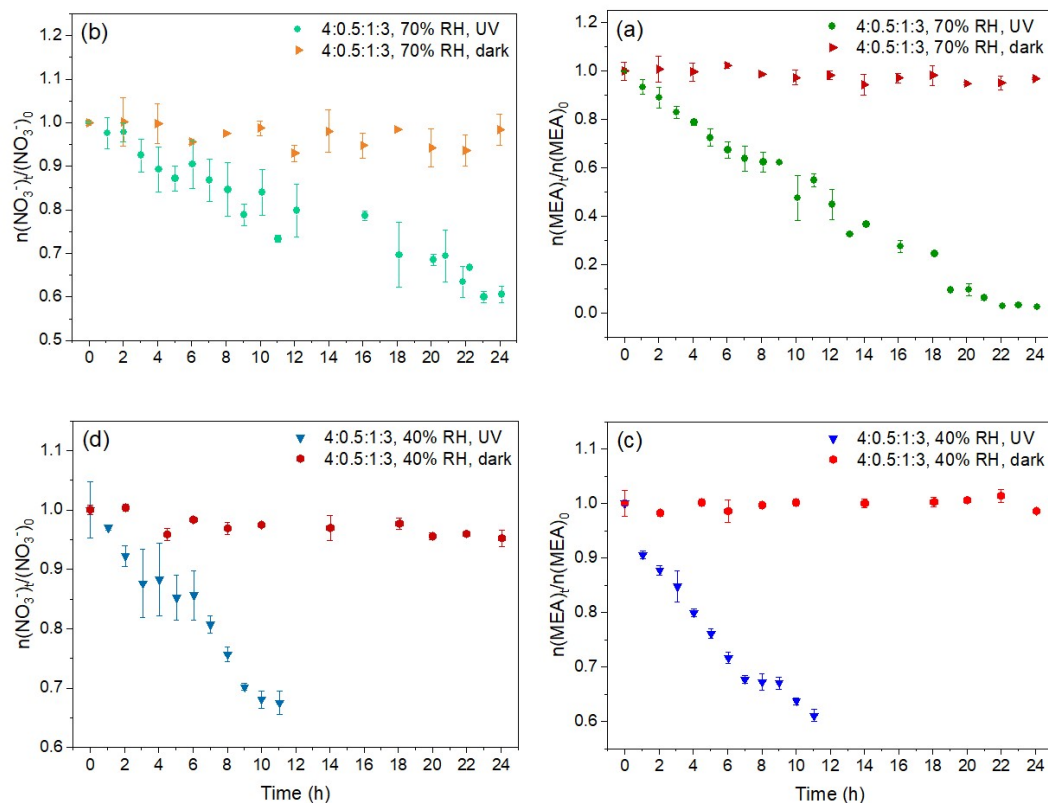
273 particles.
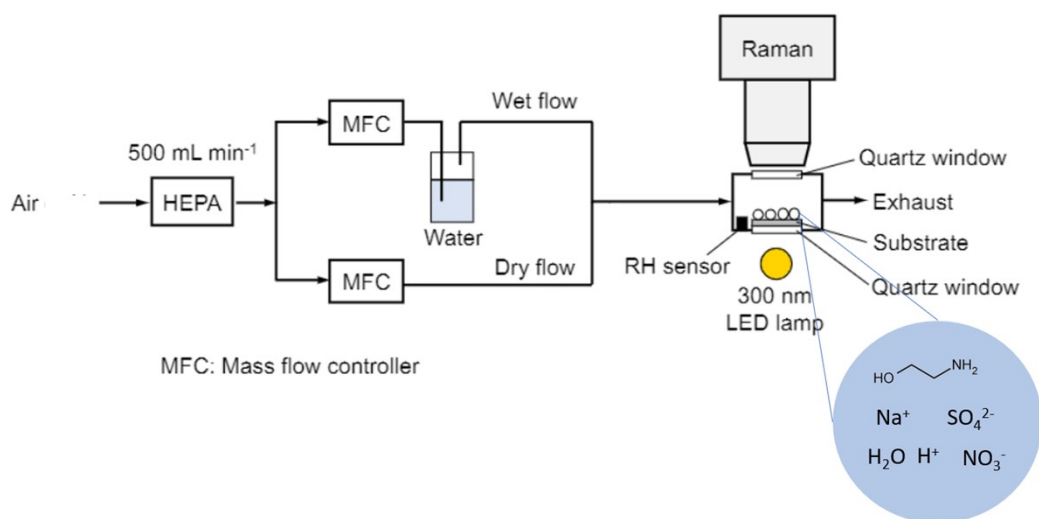
274
275 Fig. S1 Schematic of the experimental setup.
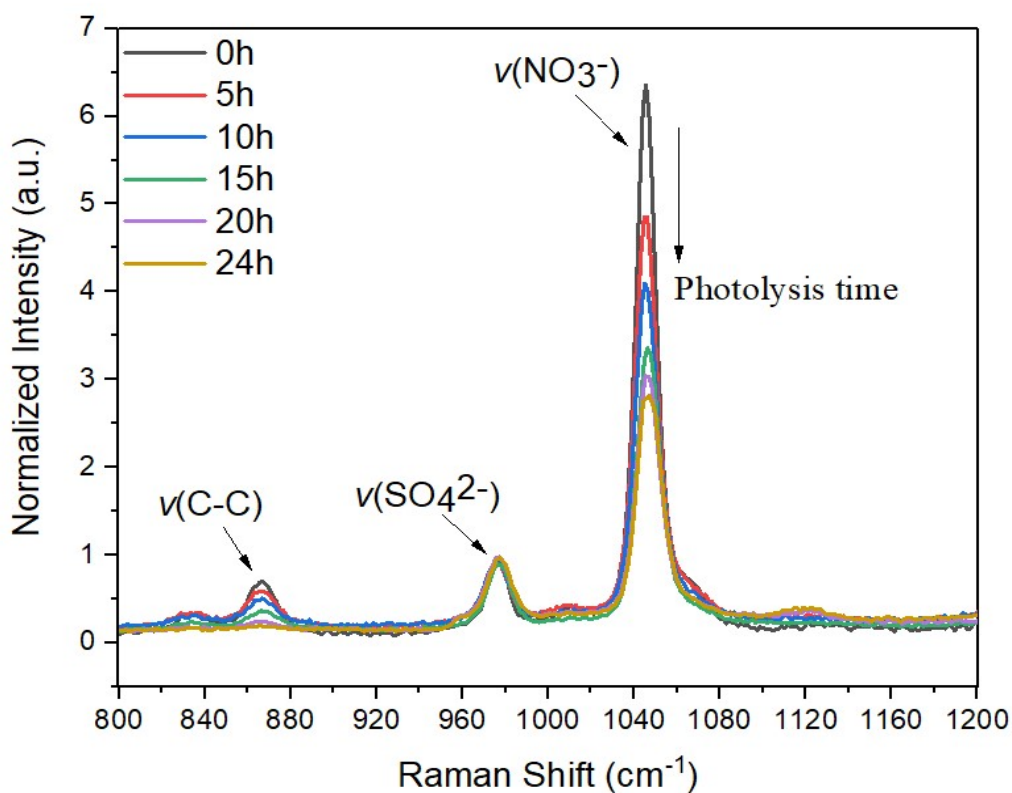
276

277 Fig. S2 Time evolution of Raman spectra for the 4:0.5:1:3 (MEA: H_2SO_4: $NaNO_3$:

278 HNO_3) particles at 70% RH.

279

280

Fig. S3 Dark control experiment for MEA: H_2SO_4: $NaNO_3$: HNO_3=4:0.5:1:3 particles. Error bars represent one standard deviation from triplicate experiments. (a) $n(NO_3^-)_t/n(NO_3^-)_0$ as a function of irradiation time under dark and UV irradiation at 70%RH; (b) $n(MEA)_t/n(MEA)_0$ as a function of irradiation time under dark and UV irradiation at 70%RH; (c) $n(NO_3^-)_t/n(NO_3^-)_0$ as a function of irradiation time under dark and UV irradiation at 40%RH; (d) $n(MEA)_t/n(MEA)_0$ as a function of irradiation time under dark and UV irradiation at 40%RH.

288

289

290
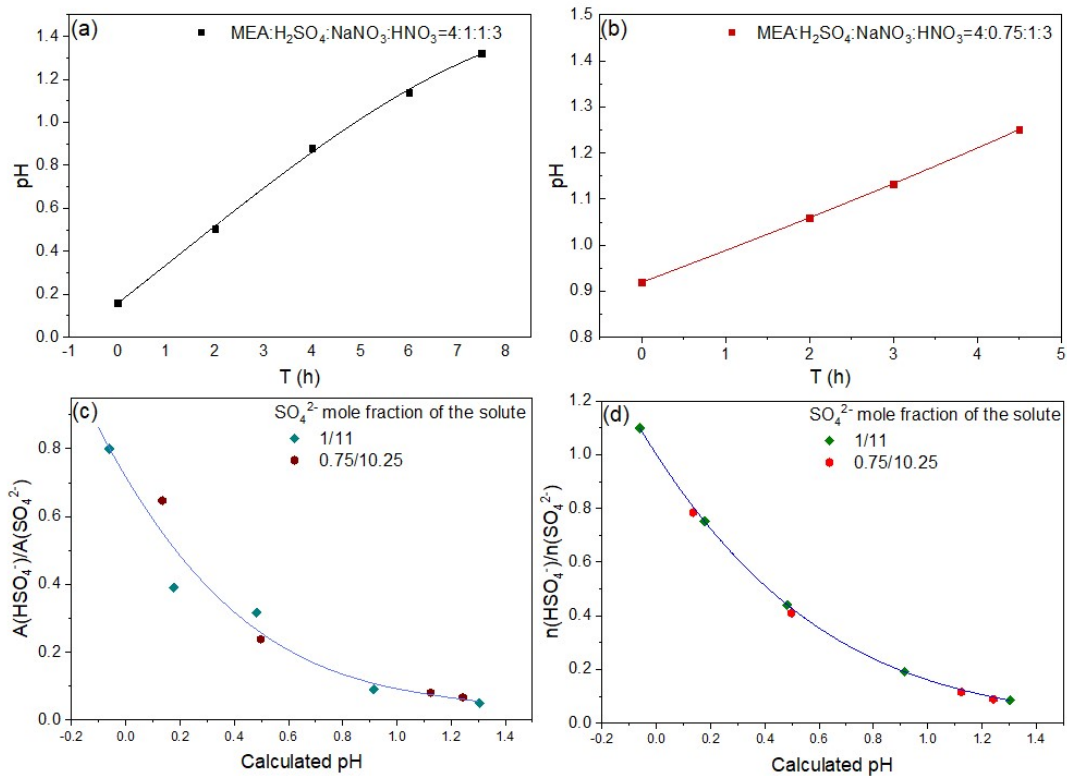
Fig. S4 (a) pH as a function of photolysis time for MEA: H_2SO_4: $NaNO_3$: HNO_3 = 4:1:1:3 particles; (b) pH as a function of photolysis time for MEA: H_2SO_4: $NaNO_3$: HNO_3=4:0.75:1:3 particles; (c) $A(HSO_4^-)/A(SO_4^{2-})$ as a function of calculated pH; (d) $n(HSO_4^-)/n(SO_4^{2-})$ as a function of calculated pH. Solution composition in (c) and (d) are listed in Table S1. The solid lines are the polynomial fittings and results are described in Eqn (S3-6).

297 **Glycolamide**
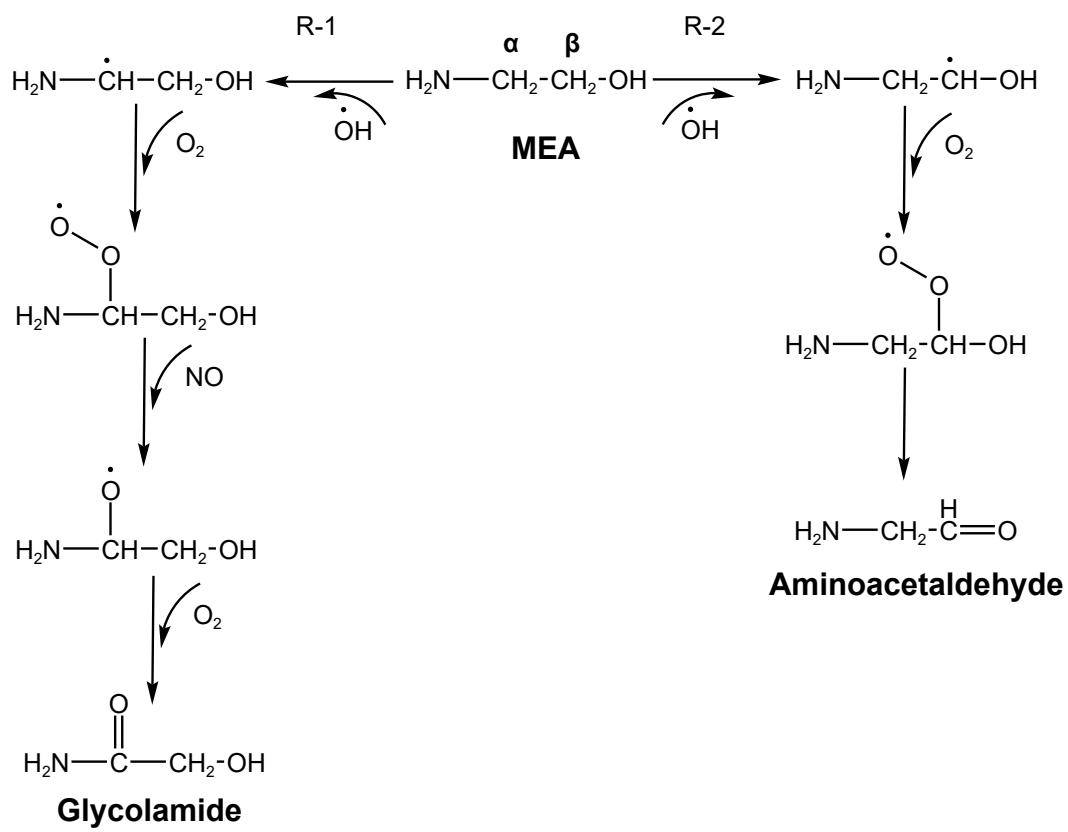
298 Fig. S5 MEA degradation pathway.
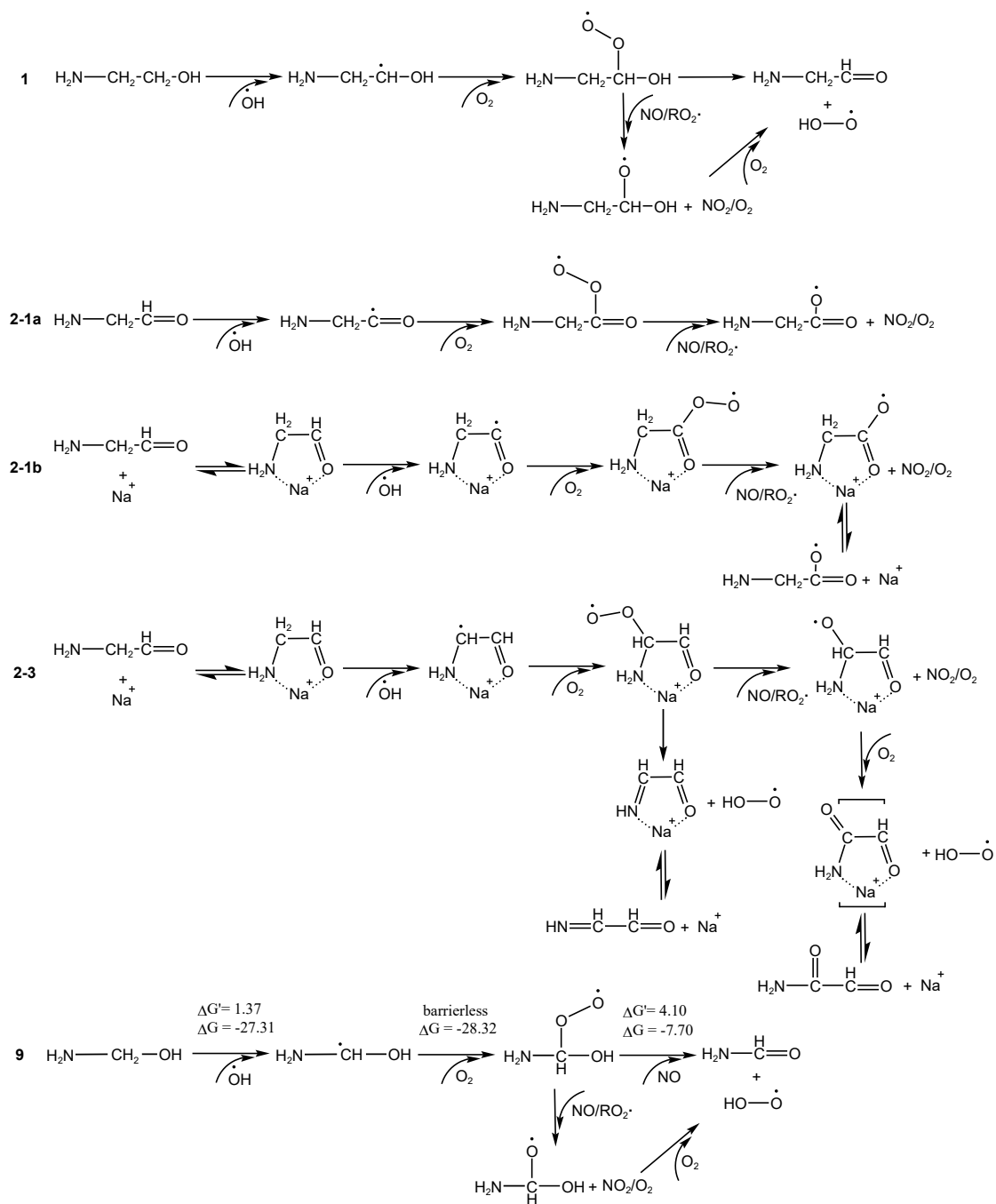
299
300

301 Fig. S6 Detailed pathways for steps 1, 2-1, 2-2, and 9 in Fig. 3.

	0h	5h	10h	15h	20h	24h
MEA:H$_2$SO$_4$:NaNO$_3$:HNO$_3$ =4:1:1:3, 70%RH						
MEA:H$_2$SO$_4$:NaNO$_3$:HNO$_3$ =4:0.75:1:3, 70%RH						
MEA:H$_2$SO$_4$:NaNO$_3$:HNO$_3$ =4:0.5:1:3, 70%RH						
MEA:H$_2$SO$_4$:NaNO$_3$:HNO$_3$ =4:0.5:1:3, 40%RH						
MEA:H$_2$SO$_4$:NaNO$_3$:HNO$_3$ =4:0.5:1:3, 55%RH						
MEA:H$_2$SO$_4$:NaNO$_3$:HNO$_3$ =4:0.5:1:3, 85%RH						

302

303 Fig. S7 Changes in particle morphologies under different experimental conditions as a

304 function of time of irradiation. Phase change of the 4:0.5:1:3 particles at 40%RH are

305 highlighted in the dashed box.
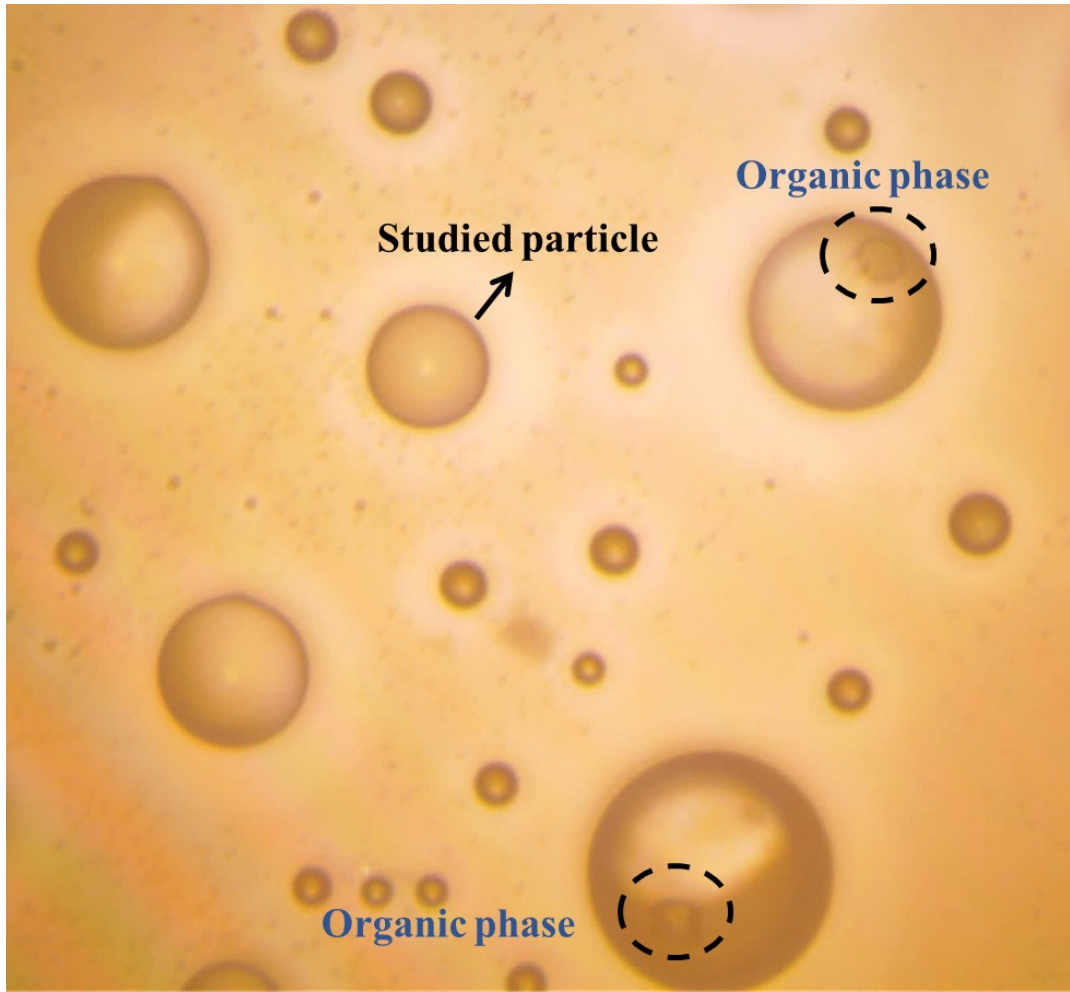
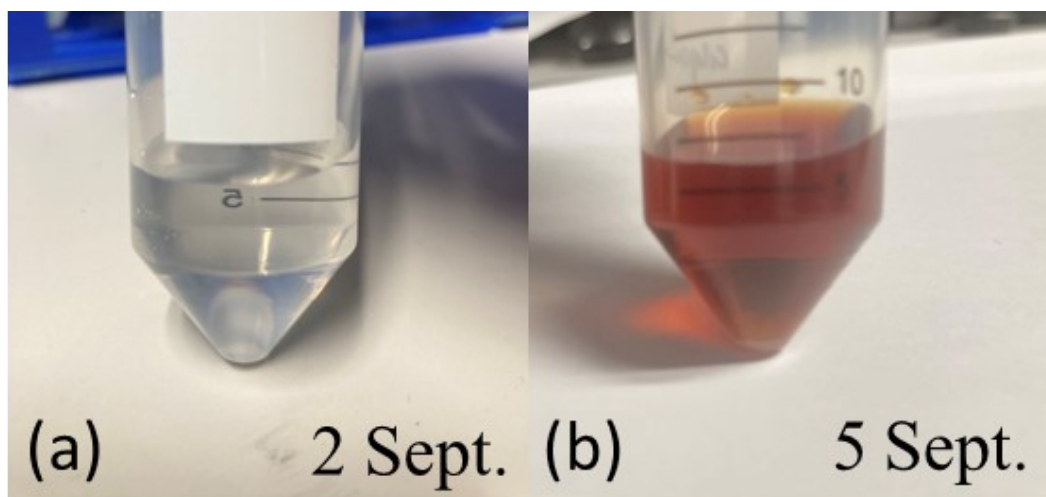Fig. S8 Morphology of the 4:0.5:1:3 particles at 85% RH after 24hr irradiation.

Fig. S9 The 4:0.5:1:3 particles on the substrate before the experiment (a), after 24hr irradiation (b) and continually supplying air without UV irradiation for another 12 hr (c) at 85%RH.

312
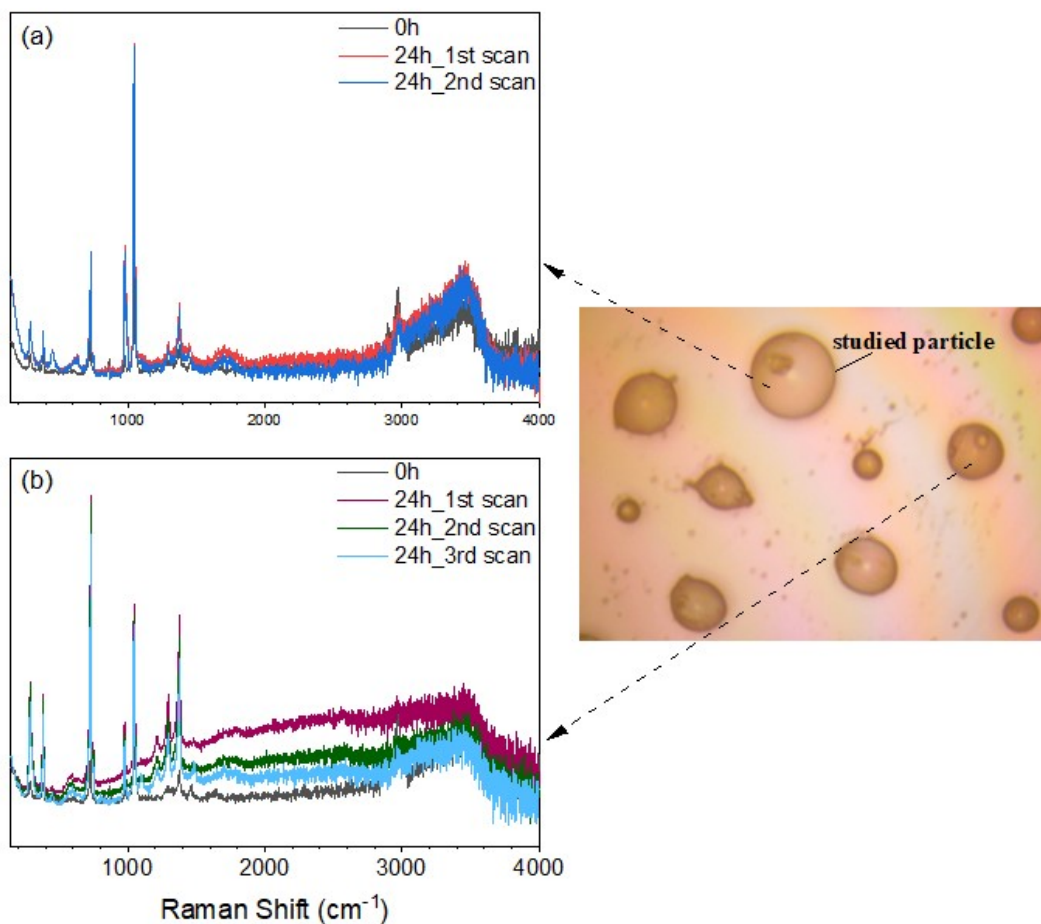
Fig. S10 Raman spectra for the liquid phase of the studied particle (a) and a neighboring particle(b) after 24hr UV irradiation. During the 24hr irradiation, no Raman laser exposure was given to particles. Raman spectra for the particle at 0hr before UV irradiation were plotted as the reference.

317

318

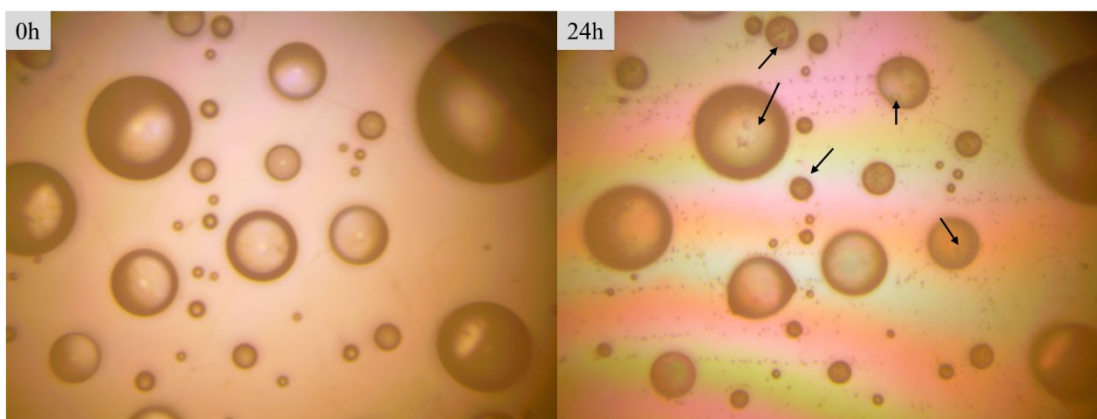Fig. S11 (a) Freshly made solution by mixing MEA, NH_2CHO, CHOCHO,

NH_2CH_2COOH, Na_2SO_4, $(NH_4)_2SO_4$ and H_2SO_4. (b) Same solution after 3 days in the

dark.

322
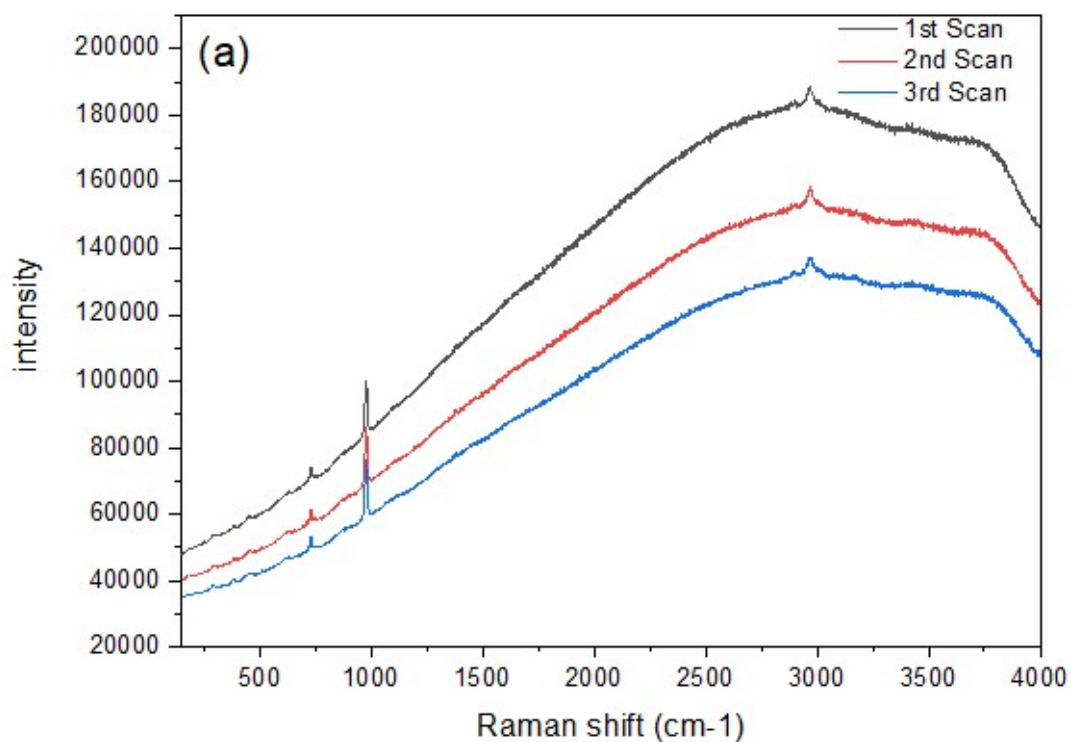
Fig. S12 Raman spectra for the particle made by the solution in Fig. S11(b).

324

325
326 Fig. S13 (a) Morphology of particles made from the solution in Fig. S11(b); (b)

327 Morphology of particles made from the solution in Fig. S11(b) after 24hr UV

328 irradiation. $NaNO_3$ was added to the solution before making particles.
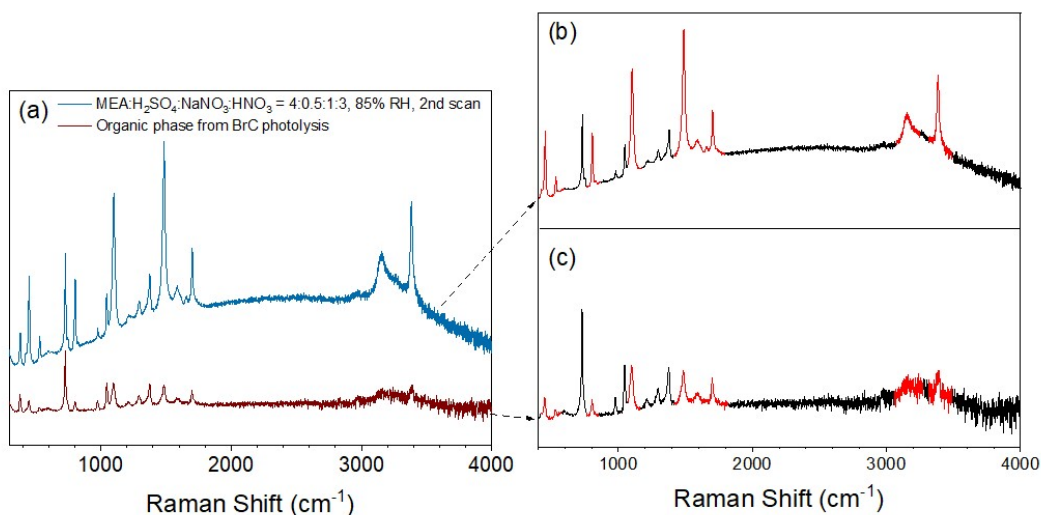
329
330 Fig. S14 (a) Detected Raman signals in the organic phase at 24 hr irradiation of the

331 4:0.5:1:3 particles at 85% RH for the second scan and in the organic phase from BrC

332 photolysis. Raman peaks of organic phase in each spectrum were highlighted in red in

333 (b) and (c).
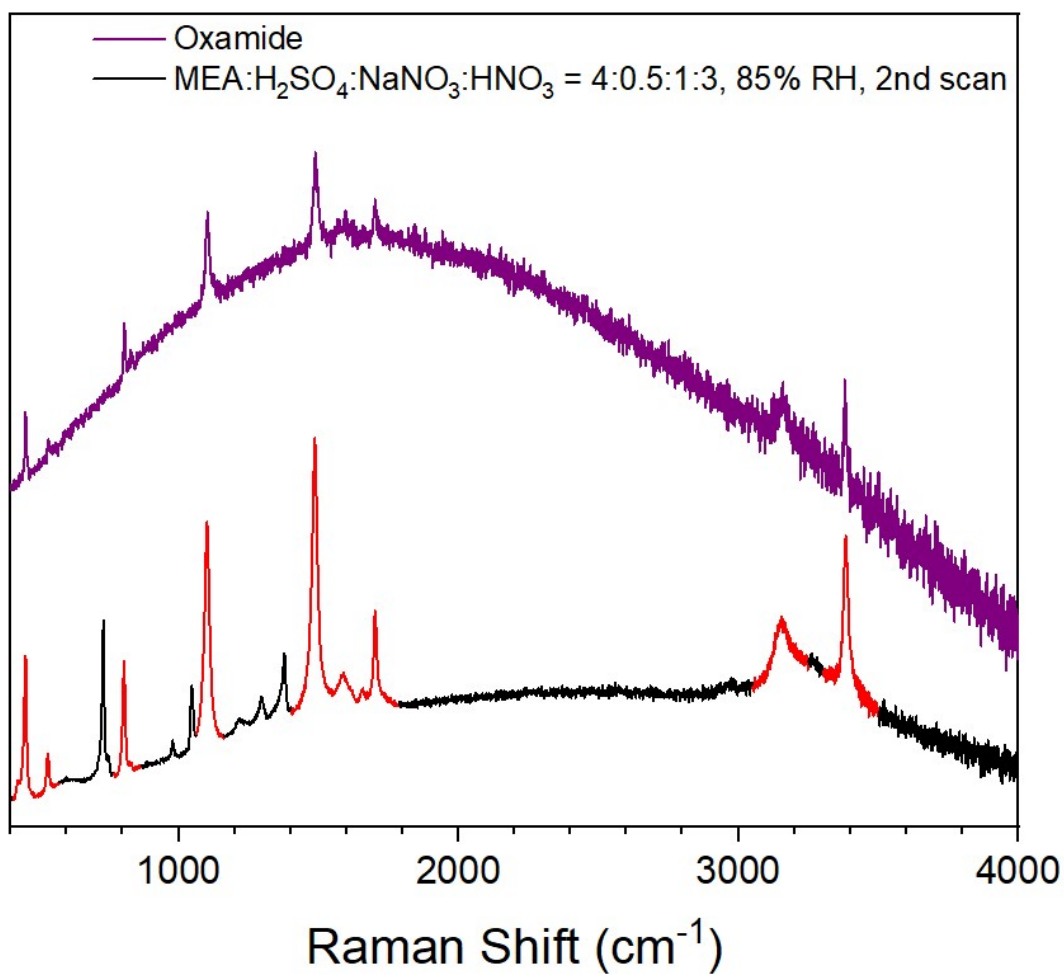
334
Fig. S15 Detected Raman signals in oxamide and in the organic phase after 24 hr

irradiation of the 4:0.5:1:3 particles at 85% RH for the second scan. Raman peaks

attributed to oxamide were highlighted in red.
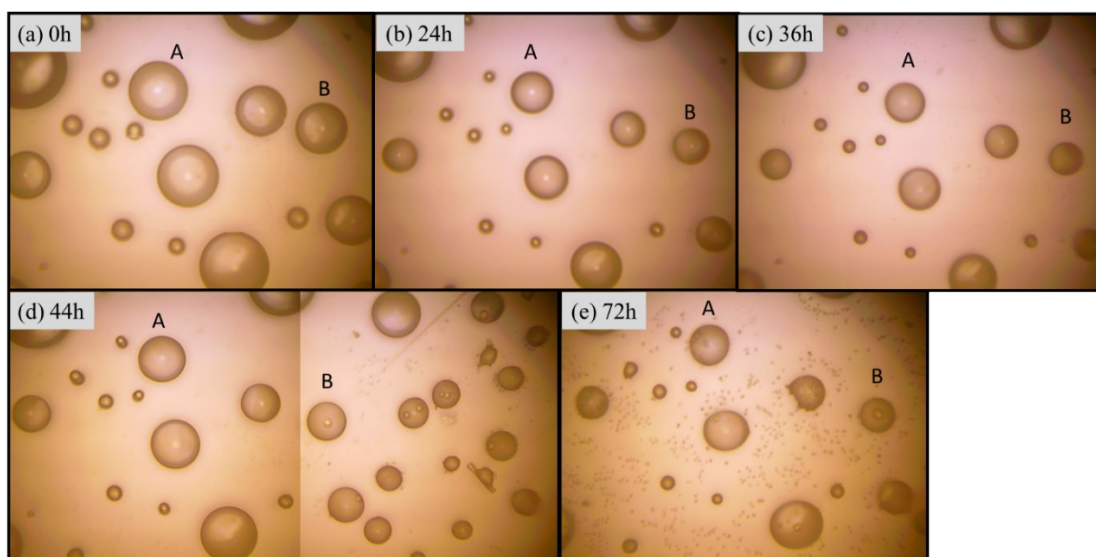
339
340 Fig. S16 Changes in morphologies of the 4:0.5:1:3 particles at 80%RH (a) Particles

341 before the experiment; (b) particles after one cycle of day-night (12hr UV+12hr dark);

342 (c) particles after the one cycle of day-night and a day (12hr UV+12hr dark +12hr UV);

343 (d) particles after the one cycle of day-night and a day + 8hr dark, photo was extended

344 by merging two photos; (e) particles after 3 cycle of day-night. A particle in the center

345 area was designated as particle A, while a particle at the periphery was designated as

346 particle B.

347

348

349

350

351

352

353

354

355 **Table S1. Raman calibration experiments using different NH_4Cl: H_2SO_4: Na_2SO_4**

356 solutions to determine $A(HSO_4^-)/A(SO_4^{2-})$ as a function of pH for MEA oxidation

357 experiments. Noted that the SO_4^{2-} mole fraction of the solute in MEA: H_2SO_4:

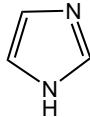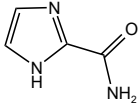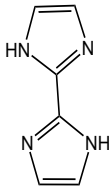358 $NaNO_3$: HNO_3 = 4:1:1:3 and 4:0.75:1:3 are 1/11 and 0.75/10.25 respectively. All

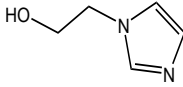| SO_4^{2-} mole fraction of the solute	NH₄Cl: H_2SO_4: Na_2SO_4	$n(HSO_4^-)/n(SO_4^{2-})$	Calculated pH
1/11	4:0.4:0.6	1.10	-0.06
	4:0.3:0.7	0.75	0.18
	4:0.2:0.8	0.44	0.48
	4:0.1:0.9	0.19	0.91
	4:0.05:0.95	0.09	1.28
	4:0.0475:0.9525	0.04	1.30
0.75/10.25	4:0.25:0.5	0.78	0.14
	4:0.15:0.6	0.41	0.50
	4:0.05:0.7	0.12	1.13
	4:0.04:0.71	0.09	1.24

359 calibration experiments were carried out at 70%RH.

360

361

362

Table S2. Compound found in MS with the m/z values and structure.

Compound	m/z	Structure
Aminoacetaldehyde (C_2H_5NO)	60.0458 82.0265(Sodication)	H_2N—CH_2-CH=O
Glyoxamide ($C_2H_3NO_2$)	74.0603	H_2N—C(=O)—CH=O
glycine ($C_2H_5NO_2$)	76.0318	H_2N—CH_2-C(OH)=O
Imidazole ($C_3H_4N_2$)	69.0445	
1H-Imidazol-2-carboxamid ($C_4H_5N_3O$)	112.02	
Biimidazole ($C_6H_6N_4$)	135.0627	
Imidazole-1-ethanol ($C_5H_8N_2O$)	113.0707	
Imidazole-4-acetaldehyde ($C_5H_6N_2O$)	111.0550	

364

365

366

367
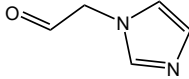
References:

1 C. Lee, C. Schmidt, J. Yoon and U. von Gunten, *Environ. Sci. Technol.*, 2007, **41**, 2056–2063.

2 Y. Chu, M. Sauerwein and C. K. Chan, *Physical Chemistry Chemical Physics*, 2015, **17**, 19789–19796.

3 M. J. Frisch, G. W. Trucks, H. B. Schlegel, G. E. Scuseria, M. A. Robb, J. R. Cheeseman, G. Scalmani, V. Barone, G. A. Petersson and H. Nakatsuji, *Inc.: Wallingford, CT, USA*.

4 Y. Zhao and D. G. Truhlar, *Theor Chem Account*, 2008, **120**, 215–241.

5 A. V. Marenich, C. J. Cramer and D. G. Truhlar, *The Journal of Physical Chemistry B*, 2009, **113**, 6378–6396.

6 H.-B. Xie, C. Li, N. He, C. Wang, S. Zhang and J. Chen, *Environ. Sci. Technol.*, 2014, **48**, 1700–1706.

7 B. Vanderhaegen, H. Neven, H. Verachtert and G. Derdelinckx, *Food Chemistry*, 2006, **95**, 357–381.

8 S. Harimurti, B. K. Dutta, I. F. B. M. Ariff, S. Chakrabarti and D. Vione, *Water Air Soil Pollut*, 2010, **211**, 273–286.

9 Y. B. Lim, Y. Tan, M. J. Perri, S. P. Seitzinger and B. J. Turpin, *Atmospheric Chemistry and Physics*, 2010, **10**, 10521–10539.

10 R. M. Moision and P. B. Armentrout, *J. Phys. Chem. A*, 2002, **106**, 10350–10362.

11 A. L. Heaton, R. M. Moision and P. B. Armentrout, *J. Phys. Chem. A*, 2008, **112**, 3319–3327.

12 R. Atkinson and J. Arey, *Chem. Rev.*, 2003, **103**, 4605–4638.

13 H. J. Chacon-Madrid, A. A. Presto and N. M. Donahue, *Physical Chemistry Chemical Physics*, 2010, **12**, 13975–13982.

14 M. Karl and P. Herckes, 61.

15 M. Yasuda, T. Tomo, S. Hirata, T. Shiragami and T. Matsumoto, *Catalysts*, 2014, **4**, 162–173.

16 B. Picquet-Varrault, R. Suarez-Bertoa, M. Duncianu, M. Cazaunau, E. Pangui, M. David and J.-F. Doussin, *Atmospheric Chemistry and Physics*, 2020, **20**, 487–498.

17 R. Atkinson and J. Arey, *Chem. Rev.*, 2003, **103**, 4605–4638.

18 J. F. Marlier, E. Campbell, C. Lai, M. Weber, L. A. Reinhardt and W. W. Cleland, *J. Org. Chem.*, 2006, **71**, 3829–3836.

19 B. Wang and Z. Cao, *J. Phys. Chem. A*, 2010, **114**, 12918–12927.

20 D. O. De Haan, L. N. Hawkins, H. G. Welsh, R. Pednekar, J. R. Casar, E. A. Pennington, A. de Loera, N. G. Jimenez, M. A. Symons, M. Zauscher, A. Pajunoja,

404   L. Caponi, M. Cazaunau, P. Formenti, A. Gratien, E. Pangui and J.-F. Doussin,
405   *Environ. Sci. Technol.*, 2017, **51**, 7458–7466.

406 21 J.-L. Chen, L. He, H. Yang, M. Ma, Q. Chen, S.-J. Wu and Z. Xiao, *Renewable*
407   *and Sustainable Energy Reviews*, 2019, **108**, 91–111.

408 22 X. Tian, Y. Chu and C. K. Chan, *Environ. Sci. Technol. Lett.*, 2022, **9**, 16–21.

409 23 R. Zhang, M. Gen, T.-M. Fu and C. K. Chan, *Environ. Sci. Technol.*, 2021, **55**,
410   5711–5720.

411 24 U. von Gunten, *Water Research*, 2003, **37**, 1443–1467.

412